ELSEVIER

Chemical Engineering Journal 129 (2007) 51–65

Chemical Engineering Journal

www.elsevier.com/locate/cej

Review

An overview of the structure and magnetism of spinel ferrite nanoparticles and their synthesis in microemulsions

Daliya S. Mathew, Ruey-Shin Juang *

Department of Chemical Engineering and Materials Science, Yuan Ze University, Chung-Li 32003, Taiwan

Received 21 July 2006; received in revised form 20 October 2006; accepted 7 November 2006

Abstract

In this review, we attempt to describe the structure of various spinel ferrites like zinc ferrite, nickel–zinc ferrite, manganese–zinc ferrite and cobalt ferrite. It also describes the important magnetic properties of these spinel ferrites. The focus then shifts to the use of microemulsions as nanoreactors for the synthesis of spinel ferrites. This work gives a short review on the various synthesis methods of spinel ferrites in microemulsions in the recent years.

Keywords: Structure; Magnetism; Synthesis; Spinel ferrites; Nanoparticles; Microemulsions

1. Introduction

Nanotechnology is the understanding and control of matter at dimensions of roughly 1–100 nm, where unique phenomena enable novel applications. The physical and chemical properties of the nanomaterials tend to be exceptionally closely dependent on their size and shape or morphology. As a result, materials scientists are focusing their efforts on developing simple and effective methods for fabricating nanomaterials with controlled size and morphology and hence tailoring their properties. An important aspect of the nanoscale is that the smaller a nanoparticle gets, the larger its relative surface area becomes. At the nanoscale, properties like electrical conductivity and mechanical strength are not the same as they are at bulk size. Its electronic structure changes dramatically, too.

Recently, the synthesis of magnetic materials on the nanoscale has been a field of intense study, due to the novel mesoscopic properties shown by particles of quantum dimensions located in the transition region between atoms and bulk solids [1]. Quantum size effects and the large surface area of magnetic nanoparticles dramatically change some of the magnetic properties and exhibit superparamagnetic phenomena and quantum tunneling of magnetization, because each particle can be considered as single magnetic domain.

Magnetic nanoparticles of spinel ferrites are of great interest in fundamental science, especially for addressing the fundamental relationships between magnetic properties and their crystal chemistry and structure. Crystal chemistry shows how the chemical composition (chemical formula), internal structure and physical properties of minerals are linked together. Spinel ferrites have been investigated in recent years for their useful electrical and magnetic properties and applications in information storage systems, magnetic bulk cores, magnetic fluids, microwave absorbers and medical diagnostics. The synthesis and magnetic structure characterization of spinel metastable nanoferrites have been investigated with much interest [2–4] and a lot of attention has been focused on the preparation and characterization of superparamagnetic metal oxide nanoparticles of spinel ferrites, $MeFe_2O_4$ (metal Me = Co, Mg, Mn, Zn, etc.) [5–10]. The rich crystal chemistry in spinel ferrite systems offers excellent opportunities for understanding and fine-tuning the superparamagnetic properties of nanoparticles by chemical manipulations.

This paper first gives an account of magnetism and a general overview of ferrites, followed by a short description to microemulsions as nanoreactors and then a mini review on the recent synthesis of spinel ferrites in microemulsion medium.

2. Magnetism in materials

Materials are classified by their response to an externally applied magnetic field. Descriptions of orientations of the mag-

* Corresponding author. Tel.: +886 3 4638800x2555; fax: +886 3 4559373.
E-mail address: rsjuang@ce.yzu.edu.tw (R.-S. Juang).

1385-8947/$ – see front matter © 2006 Elsevier B.V. All rights reserved.
doi:10.1016/j.cej.2006.11.001

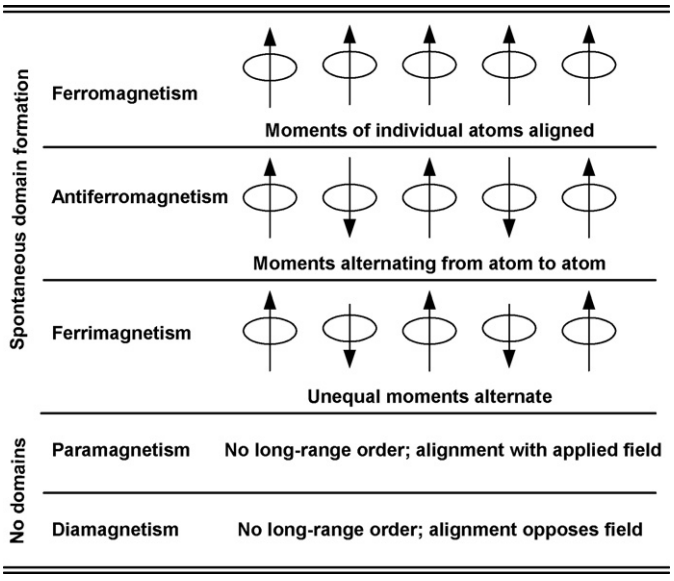

Fig. 1. Different types of magnetic behavior.

netic moments in a material help to identify different forms of magnetism observed in nature (Fig. 1). Five basic types of magnetism can be described: diamagnetism, paramagnetism, ferromagnetism, antiferromagnetism and ferrimagnetism. In the presence of an externally applied magnetic field the atomic current loops created by the orbital motion of electrons respond to oppose the applied field. All materials display this type of weak repulsion to a magnetic field known as diamagnetism. However, diamagnetism is very weak and therefore any other form of magnetic behavior that a material may possess usually overpowers the effects of the current loops. In terms of electronic configuration of materials, diamagnetism is observed in materials with filled electronic subshells where the magnetic moments are paired and overall cancel each other. Diamagnetic materials have a negative susceptibility ($\chi < 0$) and weakly repel an applied magnetic field (e.g., quartz SiO_2 and calcite $CaCO_3$). The effects of these atomic current loops are overcome if the material displays a net magnetic moment or has long-range ordering of magnetic moments [11].

All other types of magnetic behavior observed in materials are at least partially attributed to unpaired electrons in atomic shells, often in the 3d or 4f shells of each atom. Materials whose atomic magnetic moments are uncoupled display paramagnetism. Thus, paramagnetic materials moments have no long-range order and there is a small positive magnetic susceptibility ($\chi \approx 0$); e.g., montmorillonite and pyrite [11]. Materials that possess ferromagnetism have aligned atomic magnetic moments of equal magnitude and their crystalline structure allows for direct coupling interactions between the moments, which may strongly enhance the flux density (e.g., Fe, Ni and Co). Furthermore, the aligned moments in ferromagnetic materials can confer a spontaneous magnetization in the absence of an applied magnetic field. Materials that retain permanent magnetization in the absence of an applied field are known as hard magnets.

Materials having atomic magnetic moments of equal magnitude that arranged in an antiparallel fashion display antiferromagnetism (e.g., troilite FeS and ilmenite $FeTiO_2$). The exchange interaction couples the moments such that they are antiparallel therefore leaving a zero net magnetization [12]. Above the Neel temperature (T_N) thermal energy is sufficient to cause the equal and oppositely aligned atomic moments to randomly fluctuate leading to a disappearance of their long-range order. In this state the material exhibits paramagnetic behavior. Ferrimagnetism is a property exhibited by materials whose atoms or ions tend to assume an ordered but non-parallel arrangement in zero applied field below a certain characteristic temperature known as the Neel temperature (e.g., Fe_3O_4 and Fe_3S_4). In the usual case, within a magnetic domain, a substantial net magnetization results from the antiparallel alignment of neighboring non-equivalent sublattices. The macroscopic behavior is similar to ferromagnetism. Above the Neel temperature, the substance becomes paramagnetic.

Size reduction in magnetic materials resulting in the formation of single-domain particles also gives rise to the phenomenon of superparamagnetism. Briefly, superparamagnetism occurs when thermal fluctuations or an applied field can easily move the magnetic moments of the nanoparticle away from the easy axis, the preferred crystallographic axes for the magnetic moment to point along. Each particle behaves like a paramagnetic atom, but with a giant magnetic moment, as there is still a well-defined magnetic order in each nanoparticle [13].

2.1. Single-domain particles

Domains, which are groups of spins all pointing in the same direction and acting cooperatively are separated by domain walls, which have a characteristic width and energy associated with their formation and existence. The motion of domain walls is a primary means of reversing magnetization. Experimental investigation of the dependence of coercivity on particle size showed a behavior similar to that schematically illustrated in Fig. 2 [14]. It was found that the coercivity H_c increases with decreasing grain size D down to values of about 40 nm, independent of the kind of material. The increase of H_c is proportional

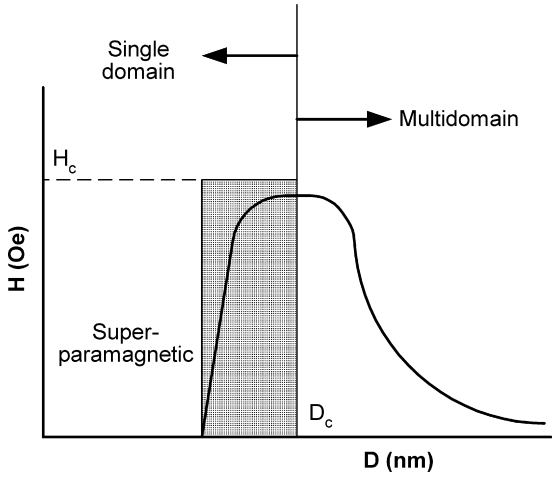

Fig. 2. Qualitative illustration of the behavior of the coercivity in ultrafine systems as the particle size changes, where H is the magnetic field amplitude (Oe) and D is the particle diameter (nm).

to 1/D. The reason for this is that in small particles the formation of a closed magnetic flux becomes energetically less favorable so that the magnetic domain size with a uniform magnetization becomes more and more identical with the grain size. This grain size is defined as the first critical size (D_c, which is characteristic of each material) where the multidomain materials change to a monodomain material. This leads to a strong increase of the coercivity (or high remanence) because a change of magnetization in this case cannot happen only by shifting the domain walls which normally requires only a weak magnetic field.

As the size of magnetic element scales below 20 nm, the transformation from ferromagnetic to superparamagnetic behavior occurs. In the superparamagnetic state of the material, the room temperature thermal energy overcomes the magnetostatic energy well of the domain or the particle, resulting in zero hysteresis. In other words, although the particle itself is a single-domain ferromagnet, the ability of an individual magnetic "dot" to store magnetization orientation information is lost when its dimension is below a threshold. Consequently, the magnetic moments within a particle rotate rapidly in unison, exhibiting the superparamagnetic relation phenomenon.

2.2. Parameters

The most commonly measured magnetic parameters are schematically illustrated in a hysteresis loop (magnetization versus field) (Fig. 3). The application of a sufficiently large magnetic field causes the spins within a material to align with the field. The maximum value of the magnetization achieved in this state is called the saturation magnetization, M_s. As the magnitude of the magnetic field decreases, spins cease to be aligned with the field and the total magnetization decreases. In ferromagnets, a residual magnetic moment remains at zero field. The value of the magnetization at zero field is called the remanent magnetization, M_r. The ratio of remanent magnetization to the saturation magnetization, M_r/M_s, is called the remanence ratio and varies from 0 to 1. The coercive field H_c is the magnitude of the field that must be applied in the negative direction to bring the magnetization of the sample back to zero. The shape of the hysteresis loop is especially of interest for magnetic recording applications, which require a large remanent magnetization, moderate coercivity and (ideally) a square hysteresis loop [15].

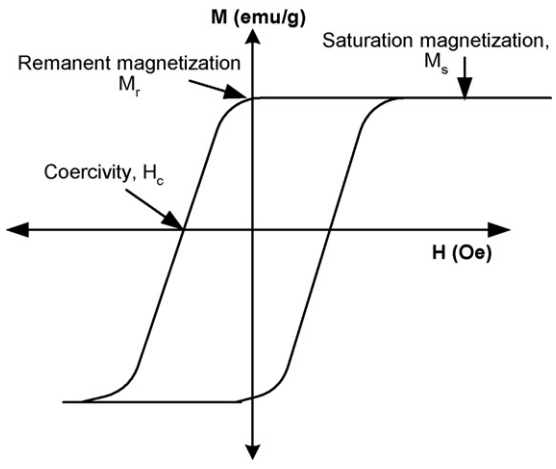

Fig. 3. Hysteresis cycle of a multidomain magnetic material, where H is the magnetic field amplitude (Oe) and M is the magnetization of the material (emu/g).

3. General overview of the structure of ferrites

The spinel ferrite structure $MeFe_2O_4$, where Me refers to the metal, can be described as a cubic close-packed arrangement of oxygen atoms, with Me^{2+} and Fe^{3+} at two different crystallographic sites. These sites have tetrahedral and octahedral oxygen coordination (termed as A and B-sites, respectively), so the resulting local symmetries of both sites are different (Fig. 4). The spinel structure contains two cation sites for metal cation occupancy. There are 8 A-sites in which the metal cations are tetrahedrally coordinated with oxygen, and 16 B-sites which possess octahedral coordination. When the A-sites are occupied by Me^{2+} cations and the B-sites are occupied by Fe^{3+} cations, the ferrite is called a normal spinel. If the A-sites are completely occupied by Fe^{3+} cations and the B-sites are randomly occupied by Me^{2+} and Fe^{3+} cations, the structure is referred to as an inverse spinel. In most spinels, the cation distribution possesses an intermediate degree of inversion where both sites contain a fraction of the Me^{2+} and Fe^{3+} cations. Magnetically, spinel ferrites display ferrimagnetic ordering. The magnetic moments of cations in the A and B-sites are aligned parallel with respect to one another. Between the A and B-sites the arrangement is antiparallel and as there are twice as many B-sites as A-sites, there is a net moment of spins yielding ferrimagnetic ordering for the crystal. The choice of metal cation and the distribution of ions between the A and B-sites therefore, offer a tunable magnetic system [16].

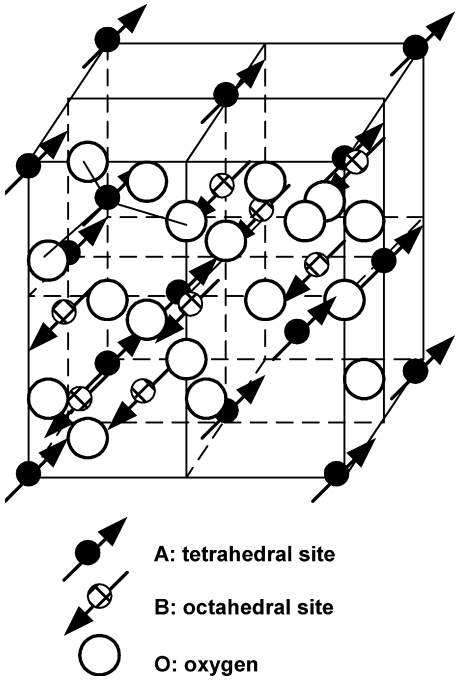

Fig. 4. Schematic of a partial unit cell and ferrimagnetic ordering of spinel ferrite structure.

According to the distribution of cations, there are the following types of ferrospinels:

(1) Normal spinel structure, where all Me^{2+} ions occupy A-sites; structural formula of such ferrites is $Me^{2+}[Fe_2{}^{3+}]O_4{}^{2-}$. This type of distribution takes place in zinc ferrites $Zn^{2+}[Fe^{2+}Fe^{3+}]O_4{}^{2-}$.
(2) Inversed spinel structure, where all Me^{2+} are in B-positions and Fe^{3+} ions are equally distributed between A and B-sites: structural formula of these ferrites are $Fe^{3+}[Me^{2+}Fe^{3+}]O_4{}^{2-}$. Magnetite Fe_3O_4, ferrites $NiFe_2O_4$ and $CoFe_2O_4$ have inversed spinel structure.
(3) Mixed spinel structure, when cations Me^{2+} and Fe^{3+} occupy both A and B-positions; structural formula of this ferrite is $Me_{1-\delta}{}^{2+}Fe_\delta{}^{3+}[Me_\delta{}^{2+}Fe_{2-\delta}{}^{3+}]O_4{}^{2-}$, where δ is the degree of inversion. $MnFe_2O_4$ represent this type of structure and has an inversion degree of $\delta = 0.2$ and its structural formula therefore is $Mn_{0.8}{}^{2+}Fe_{0.2}{}^{3+}[Mn_{0.2}{}^{2+}Fe_{1.8}{}^{3+}]O_4{}^{2-}$. Mn–Zn ferrites also have a mixed spinel structure (Zn^{2+} prefers to occupy A-sites) $Zn_x{}^{2+}Mn_y{}^{2+}Fe_{1-x-y}{}^{3+}[Mn_{1-x-y}{}^{2+}Fe_{1+x+y}{}^{3+}]O_4{}^{2-}$, where $\delta = 1 - x - y$.

Magnetic properties of ferrites have been explained by Neel [17], who postulated that magnetic moments of ferrites are a sum of magnetic moments of individual sublattices. In the ferrospinels these are: sublattice A consisting of cations in tetrahedral positions and sublattice B with cations in octahedral positions. Exchange interaction between electrons of ions in these sublattices has different value. Usually interaction between magnetic ions of sublattices A and B (A–B interaction) is the strongest. A–A interaction is almost ten times weaker and B–B interaction is the weakest. The dominant A–B interaction leads to complete or partial (non-compensated) antiferromagnetism (ferrimagnetism) [17].

In the inversed ferrites one half of Fe^{3+} is placed in A-sites and another half in B-sites. Their magnetic moments are mutually compensated and the resulting moment of the ferrite is due to the magnetic moments of bivalent cations Me^{2+} in the B-positions (Fig. 5a).

Magnetization of $MnFe_2O_4$ which has inversion degrees $\delta = 0.2$ is described in Fig. 5b. Substitution of Mn^{2+} with Zn^{2+} leads to introduction of non-magnetic Zn^{2+} ions into A-sites, thus increasing the saturation magnetization, σ_s. Increasing x up to 0.4 (at 0 K) leads to linear increase in magnetization and is described in Fig. 5c [18].

For higher Zn concentrations ($x > 0.4$–0.5) ferrite becomes normal spinel. It means that there are no more Mn^{2+} in B-sites and no more Fe^{3+} in A-sites. For $x > 0.4$, the A–B exchange interaction weakens and there is an increase in the role of B–B interaction. Due to this, magnetic moments of a part of Fe^{3+} ions (which are now only in B-position) becomes reversibly oriented which leads to the decrease of the total magnetic moment in ferrites. Higher the temperature, greater is the relative effect of the A–B exchange weakening due to the thermal fluctuations, resulting in decreased magnetization [19].

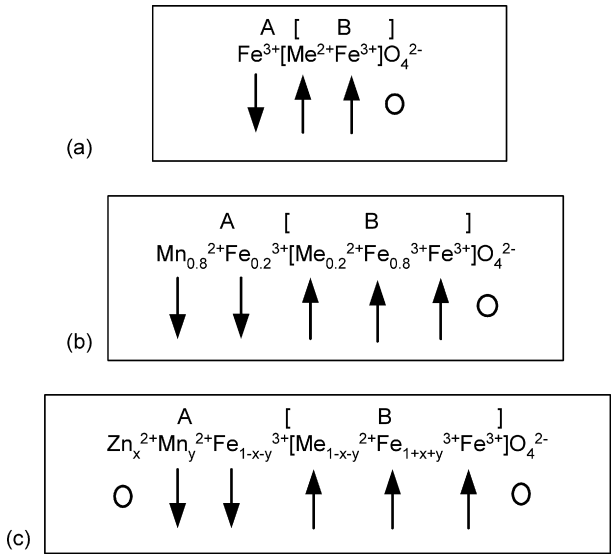

Fig. 5. Cation distribution in spinel ferrites: (a) inverted ferrites, (b) manganese ferrites and (c) zinc manganese ferrites.

3.1. Classification and applications

Magnetic materials are grouped into two types, soft and hard. This is the classification based on their ability to be magnetized and demagnetized, not their ability to withstand penetration or abrasion. Soft materials are easy to magnetize and demagnetize, so are used for electromagnets, while hard materials are used for permanent magnets. They can also be classified based on their coercive field strength into soft and hard materials. With soft magnetic materials the hysteresis loop is small (low coercive field strength, independent of magnetic field amplitude); with permanent magnets however it is large (high coercive field strength). Table 1 gives a comparative account of both types.

$H_c < 10$ A/Cm: soft magnetic;
$H_c > 300$ A/Cm: hard magnetic (permanent magnets).

Hard ferrite magnets are made in two different magnetic forms—isotropic and oriented. Isotropic magnets are formed to desired shapes, sintered and then magnetized. These exhibit a modest magnetic field and find applications in cycle dynamos

Table 1
The comparative properties of soft and hard magnetic materials

Soft magnetic	Hard magnetic
High saturation magnetization (1–2T)	High saturation magnetization (0.3–1.6T)
Low coercivity (H_c)	High coercivity
High permeability	Not important, but low
Low anisotropy	High anisotropy
Low magnetostriction	Not important
High Curie temperature (T_c)	High T_c
Low losses	High-energy product
High electrical resistivity	Not important

and ring magnets. Oriented magnets are formed to shape under a strong magnetic field and then sintered. These exhibit a very strong magnetic field and find applications in loudspeakers, magnets of two wheelers like scooters, etc. [20].

3.2. Soft ferrites

Soft ferrites are ceramic electromagnetic materials, dark gray or black in appearance and very hard and brittle. The magnetic properties of soft ferrites arise from the interactions between metallic ions occupying particular positions relative to the oxygen ions in its spinel crystalline structure. The magnetic domain theory suggests these interactions create magnetic domains, which are microscopic magnetized regions within the material. When no magnetizing force is present the magnetic domains are random and the net flux contribution is zero even though local domains are fully magnetized. When a magnetizing force is present the magnetic domains align in the direction of the magnetizing force resulting in a large net flux contribution. Soft ferrites are also semiconductors, meaning, they are somewhere between conductors and insulators in their ability to conduct electron flow through the material.

In inductor cores, transformer cores and other applications, electromagnetic materials are required to operate at high frequencies. The advantages, soft ferrites have over other electromagnetic materials include their inherent high resistivity which results in low eddy current losses over wide frequency ranges and high permeability and stability over a wide temperature range. These advantages make soft ferrites paramount over all other magnetic materials [21]. The general properties and applications of hard and soft magnetic materials are given in Table 2.

3.3. Advantage over other magnetic materials

Most other technologically useful magnetic materials such as iron and metallic alloys have low electrical resistivity. This makes them useless for applications at high frequencies, for example, as inductor cores in TV circuits. The problem is that their low electrical resistivity allows induced currents (called eddy currents) to flow within the materials themselves, thereby producing heat. This is wasted energy and the heat is often a serious problem. Thus, the materials become inefficient as they waste energy, the more so as the frequency gets higher. However, ferrites can perform much better at high frequencies because they have high electrical resistivity. High permeability and time/temperature stability are important additional characteristics, which have widened the use of ferrites into high frequency and wide-band transformers, quality filter circuits, adjustable inductors, delay lines and other high-frequency electronic circuitry. At high frequencies the use of ferrites is relatively more routine as compared to that of other circuit components whose performance needs improvement. An important factor in choosing ferrites is that they are generally cheaper than magnetic metals and alloys. Ferrites are the best core material choice for frequencies from 10 kHz to a few hundred MHz when one requires the combination of low cost, high Q (inductor quality), high stability and low volume. Furthermore, no other magnetic material has magnetic and mechanical parameters as flexible as those of ferrites.

4. Reverse micelles as microreactors

Spinel ferrite nanoparticles have been synthesized by a wide variety of methods including gas condensation, aerosol

Table 2
Properties and applications of hard and soft magnetic materials

Material	General properties and application
(a) Hard magnetic materials	
Aluminium–nickel–cobalt alloy (ALNICO), sometimes with copper and titanium	Magnets can be cast into complex shapes and perform well at high temperatures Used in applications such as instruments and meters that requires very stable temperature properties like electronic ignition systems, generators, vending machines, etc.
Rare-earth alloys (samarium)	High magnetic strength Used in wrist watches and medical implants
Neodymium–iron–boron alloys	Very low magnetic strength Used in low weight requirement applications
Hard ferrite–barium and strontium ferrite	Low cost Widespread use, including electronic applications
(b) Soft magnetic materials	
Iron with 3–4% silicon	AC motors, generators and transformers
Metallic glass-combinations of Fe, Co, Ni, B and Si	Low energy loss Use in power transformers, magnetic sensors and recording equipment
Nickel–iron alloys	Low permeability applications Used in telecommunications, aeronautical, aerospace engineering, cryogenic engineering (liquefied natural gas tankers), etc.
Hard ferrite–iron, nickel and cobalt ferrite	Low electrical conductivity reduces eddy current losses Used in high-frequency applications

reduction, chemical precipitation, sol–gel processing, thermal decomposition of organometallic precursors and continuous hydrothermal processing [22–29]. Although these methods are able to produce nanoscale ferrites, often the quality of the nanoparticles is poor in many cases (a large size distribution is reported and size control is arbitrary). In many of these procedures size variation is achieved through post-synthesis annealing at various temperatures. It was demonstrated that although nanoparticle size changes according to the annealing temperature, the cation distribution between A and B lattice sites is affected by annealing temperature [28]. Due to the ferrimagnetic nature, the magnetic properties of the spinel ferrites are highly dependent upon the distribution of cations between the A and B-sites. When annealing temperature is used to control nanoparticle size, a direct correlation between size effect and magnetic response is not possible due to the extra variable of cation re-distribution. If multiple sizes are produced through the synthesis without thermal annealing or without varying thermal annealing temperature, often large changes in the synthesis procedure are needed [16].

In order to correlate size effects with changes in magnetic properties it is critical to have a synthesis method that allows for control over the nanoparticle size and yields nanoparticles with a narrow size distribution [8]. Microemulsion approach is suitable for such purposes. Microemulsion procedures have been commonly used over the past 20 years to form high-quality metal and semiconductor nanoparticles with a small size distribution [30–33]. Furthermore, by minor adjustments to the synthesis conditions, size control is readily achievable. Microemulsion methods can be classified into normal micelle methods also called oil-in-water (o/w) methods and reverse micelle methods also referred to as water-in-oil (w/o) methods. In both cases surfactants are used and their concentration is above the critical micelle concentration (CMC).

4.1. Formation of microemulsions

Microemulsions consist of, at least, a ternary mixture of water, a surfactant or a mixture of surface-active agents and oil. Depending on the proportion of suitable components and hydrophile–lypophile balance (HLB) value of the surfactant used, the formation of microdroplets can be in the form of oil-swollen micelles dispersed in the aqueous phase or water-swollen micelles dispersed in oil. It is known that the flexibility of the surfactant films, presence of additional stabilizing agents and concentration of the reactants influence the final size of the product particles irrespective of the size of microdroplets [34]. The shape of micellar aggregates and the formation of microemulsion can be controlled and understood from the packing parameter of emulsifier molecule in the micellar assembly v/al, where v is the emulsifier hydrocarbon volume, a the polar head area and l is the fully extended chain length of the emulsifier. When the ratio v/al is larger than unity, the aggregate curvature will be towards water. This corresponds to a situation where the oil is penetrating the emulsifier tails and/or the electrostatic repulsion between the charged head group is low. When the ratio is less than unity we have a situation where the electrostatic repulsion is larger and/or the oil is not penetrating the emulsifier tails. Spherical direct micelles are formed when the packing parameter is less than 1/3. The limiting values for packing parameters for cylinders and planer bilayers are 0.5 and 1, respectively.

Reverse micellar structures are formed within the right solvent when the packing parameter is greater than 2 (cylinders up to $v/al > 2$ and the spherical micelle when $v/al > 3$). When oil is solubilized in hydrophilic micelles or water in hydrophobic micelles, one can observe the formation of o/w microemulsions for $v/al < 1$; or w/o microemulsions for $v/al > 1$. When $v/al \approx 1$, lamellar phases or bicontinuous microemulsions are observed [35]. The surfactant-covered water pools offer a unique microenvironment for the formation of nanoparticles. They not only act as microreactors for processing reactions but also exhibit the process aggregation of particles because the surfactants could adsorb on the particle surface when the particle size approaches to that of the water pool. As a result, the particles obtained in such a medium are generally extremely fine and monodisperse [36]. Inverse microemulsion droplets, however, are slightly polydisperse due to less strict transformation of monomer to assembly form. The microemulsion is a thermodynamically stable phase and therefore the polydispersity is an equilibrium property. The droplets collide, form transient aggregates and then revert to isolated droplets. Aggregate lifetimes are typically of the order of microseconds.

The dynamics of the exchange of solute between micelles and the continuous phase is characterized by the rate constant for entry of the solute into the micelle. This process is diffusion controlled, as is the entry of emulsifier molecules into the micelle. Under certain critical conditions, molecules can be transported from one droplet to another without going through the continuous phase. A possible process involves collisions and transient merging of the droplet cores. At low concentration of the dispersed phase, the dispersion is mostly composed of identical spherical isolated droplets. At higher concentrations, the structure of the system depends on the interactions between droplets. If they are repulsive, the collisions are very short and no overlapping between interfaces of colliding droplets occurs. If the interactions are attractive, the duration of collisions increases, and transient clusters of droplets are formed. Interface overlap occurs during collisions, allowing exchange between touching droplets. These exchanges are achieved by hopping of ions or molecules through the interfaces, or by transient opening of these interfaces with communication between the water cores of the droplets [37].

The transfer of inorganic salts in reverse (w/o) microemulsions has received considerable attention for preparing semiconductor and metal particles [38,39]. One of the powerful techniques for obtaining the ultrafine particles is based on the use of microemulsions as microreactors in order to control the growth of the particles [30,39]. The size of microemulsion droplets can be modified in the range 5–50 nm by varying the relation of the components of the microemulsion or by varying the microemulsion itself. Monodispersity of particles and stabilization of particles are very important criteria in controlled synthesis.

5. Nanoparticle synthesis in microemulsions

Metallic nanoparticles are obtained by simple mixing of two water-in-oil microemulsions, one containing a salt or a complex of metal and the other containing a reducing agent, such as sodium borohydride or hydrazine [30,40]. Due to their small size, the droplets are subject to Brownian motion. They collide continuously and result in the formation of dimmer's and other aggregates. These aggregates are short lived and rapidly disintegrate into droplets of the original size. As a result of the continuous coalescence and decoalescence process, the content of the water pools of the two microemulsions will be distributed evenly over the entire droplet population and reaction will occur in the droplets (nucleation and growth). Inorganic particles in the same size range as the water droplets of the starting microemulsions will eventually form. A schematic picture of this process is represented in Fig. 6 [41].

The nanoparticles formed are often amorphous [42]. However, Pileni and co-workers [42,43], who has pioneered the area, has shown that crystalline nanoparticles can be obtained by proper choice of conditions, and in particular, by using an anionic surfactant with a counterion, Me^{+} or Me^{2+}. The dynamic exchange of reactants such as metallic salts and reducing agents between droplets via the continuous oil phase is strongly depressed due to the restricted solubility of inorganic salts in the oil phase. This is the reason why the attractive interactions between the droplets play a dominant role in the particle nucleation and growth in w/o microemulsion reaction medium.

The control of size of the nanoparticles formed via the microemulsion route is an important issue that has triggered a lot of attention. The size of the water pools of the microemulsion is a function of the water-to-oil ratio used in the formulation, often denoted W_0. For commonly used surfactant AOT (sodium bis(2-ethylhexyl) sulfosuccinate), the droplet radius, R_d, can be directly obtained from the W_0 value by the relationship $R_d = 0.175W_0$ [44].

Many groups have tried to establish correlations between the size of the aqueous droplets of the starting microemulsions and the resulting inorganic particles. In some cases, such as for silver sulfide [45] and sulfated zirconia [46], both prepared in AOT-based microemulsions, there is an almost linear correlation between the W_0 value and the size of the resulting nanoparticles. However, there are hardly any cases showing a straightforward correlation between the droplet and the particle sizes. The issue of particle size control in microemulsion-based synthesis is intriguing and important. A range of recent experimental findings can be summarized as follows [47]:

1. Particle size increases with reactant concentration.
2. Particle size decreases if the concentration of one of the reactants increases far beyond the concentration of the other reactant.

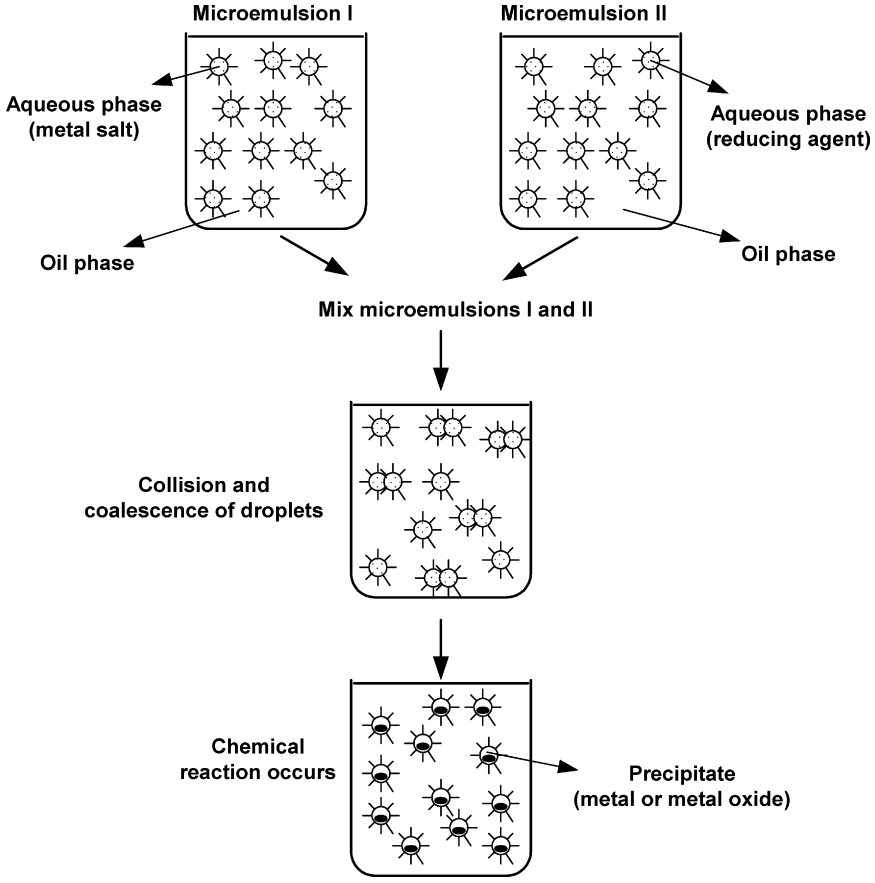

Fig. 6. Proposed mechanism for the formation of metal particles by microemulsion approach.

3. Particle size increases with an increase in surfactant film flexibility. The film flexibility can be increased by several means: incorporating an alcohol as co-surfactant, decreasing the oil molecular weight, approaching the instability border of the microemulsion, etc.
4. Particle size may increase with an increase in microemulsion droplet size.

The experimental results correlate rather well with results from Monte Carlo computer simulations made by Lopez-Quintela's group [48–50]. The Monte Carlo simulations were made under the assumption that the chemical reaction occurring in the microemulsion droplets is much faster than the exchange of materials within the droplets. If the chemical reaction is slow compared to the exchange rate, a pseudophase model can instead be used to explain the growth kinetics [51].

5.1. Zinc ferrites

Bulk $ZnFe_2O_4$ is a normal spinel form with $\delta = 1$ (corresponding to the formula $(A_\delta B_{1-\delta})[A_{1-\delta}B_\delta]_2O_4$), where δ is the inversion parameter, round and square brackets denote the tetrahedral (A-sites) and octahedral (B-sites) sites, respectively. The diamagnetic Zn^{2+} ions occupy only A-sites, as a result all Fe^{3+} ions are in B-sites and are coupled between each other via superexchange pathway through A-sites. The B–B interactions being very weak, the normal spinel $ZnFe_2O_4$ shows long-range antiferromagnetic ordering at $T_N = 9$–11 K [52,53]. The magnetization has been found to increase with grain size reduction. This feature is generally associated with the increase of the cation inversion and with the diminution of the size of the grains [9,54]. Modifying the properties of one material by coating it with another type of material has been a popular approach. In the case of coating magnetic oxide particles with silica, various routes have been investigated. Aggregation of small colloids [55], condensation of silica oligomers produced by solubilization of silica particles in a highly basic medium [56], hydrolysis of silicon alkoxide [57] and the microemulsion method [58]. With the first three processes, it is very difficult to obtain well-designed silica nanoparticles in the range from 5 to 100 nm, whereas a water-in-oil microemulsion route provides a unique environment to synthesize novel inorganic magnetic materials with interesting designs and/or specific properties resulting in non-aggregated nanoparticles.

One of the problems with the microemulsion process remains the effect of the reactants and products on the stability domain of the microemulsions, particularly the metal concentration in the aqueous pseudophase used for precipitation reactions [58]. A colloidal suspension (ferrofluid) method was used to synthesize nanoparticles, thus avoiding the classical precipitation process [59]. The colloidal suspension, used as a starting component of the aqueous pseudophase allows one to increase the metal concentration without destabilizing the microemulsion. In this case, non-stoichiometric nanoparticles of zinc ferrites were prepared using the co-precipitation process. The low-temperature w/o microemulsion technique was used to prepare spherical silica nanoparticles with a $ZnFe_2O_4$ core. This study proved that by using a stable colloidal solution as an aqueous pseudophase it is possible to prepare designed oxide nanoparticles. It was believed that the magnetic properties of the nanoparticles at low temperature were essentially governed by the interface particle habitat. This work gives one of the preliminary ideas on the control for the design of nanoparticles, the concept of very stable "nanoreactors" or "nanodroplets", an essential ingredient for the formation of core–shell nanoparticles. The SEM micrographs of the powders are presented in Fig. 7 (5a–d in the original article [59], where a, b, c and d refer to the AOT, AOT/Brij 30, Brij 30 and SDS/propanol in *n*-heptane microemulsions, respectively). In Fig. 7(5a), the silica particles appear shapeless in the microemulsion. In Fig. 7(5b and c), the silica nanoparticles consisted of an arrangement of relatively uniform particles. The diameter of silica in this case was in the range 40–60 nm. The system that showed the most uniform particle size distribution and the particle with the most perfect spherical shape was Fig. 7(5b) (surfactant phase was a mixture of AOT and Brij 30). These silica nanoparticles with a ferrite core are potentially useful photocatalytic materials. Another interest is the formation of nanostructured materials by using colloidal crystals as a template, which has potential applications in advanced catalysis, where the hierarchical porosity combines efficient transport and high surface area.

5.2. Nickel–zinc ferrites

Nickel–zinc ferrites are magnetic materials that are much used in the modern electronics industry. This is primarily due to their high electrical resistivities, which implies low eddy current losses that become significant at higher frequencies of electromagnetic fields. Nickel–zinc ferrites also exhibit high values of saturation magnetization and magnetic permeability, together with high mechanical strength, good chemical stability, low coercivities and low dielectric losses.

Current interest in making nanosized Ni–Zn ferrite particles is to reduce energy losses associated with bulk powders. Also more electronic applications require these materials be pressed into larger shapes with near theoretical density, which is difficult to obtain if the particles have a wide size distribution. The synthesis of nanoscale Ni–Zn ferrites was carried out successfully at room temperature without any further processing [60]. Their study employed the surfactant system AOT/isooctane to form the reverse micelle at room temperature. Most of the times the nanoparticles produced using reverse micelles require firing or calcination to produce the desired product, but this room temperature method did not require a firing step. The Ni–Zn ferrites produced by this method had a particle size of approximately 7 nm.

Another microemulsion used in the preparation of Ni–Zn ferrite nanoparticles was CTAB/1-hexanol/water system. Sulfates salts of nickel and zinc were the reactants and tetramethylammonium hydroxide was used as the precipitating agent [61]. In this case the amount of precipitating agent used was shown to play a crucial role in the process of synthesizing the nanosized Ni–Zn ferrite particles. If the amount of precipitating agent was less than the stoichiometric amount needed to precipitate the pre-

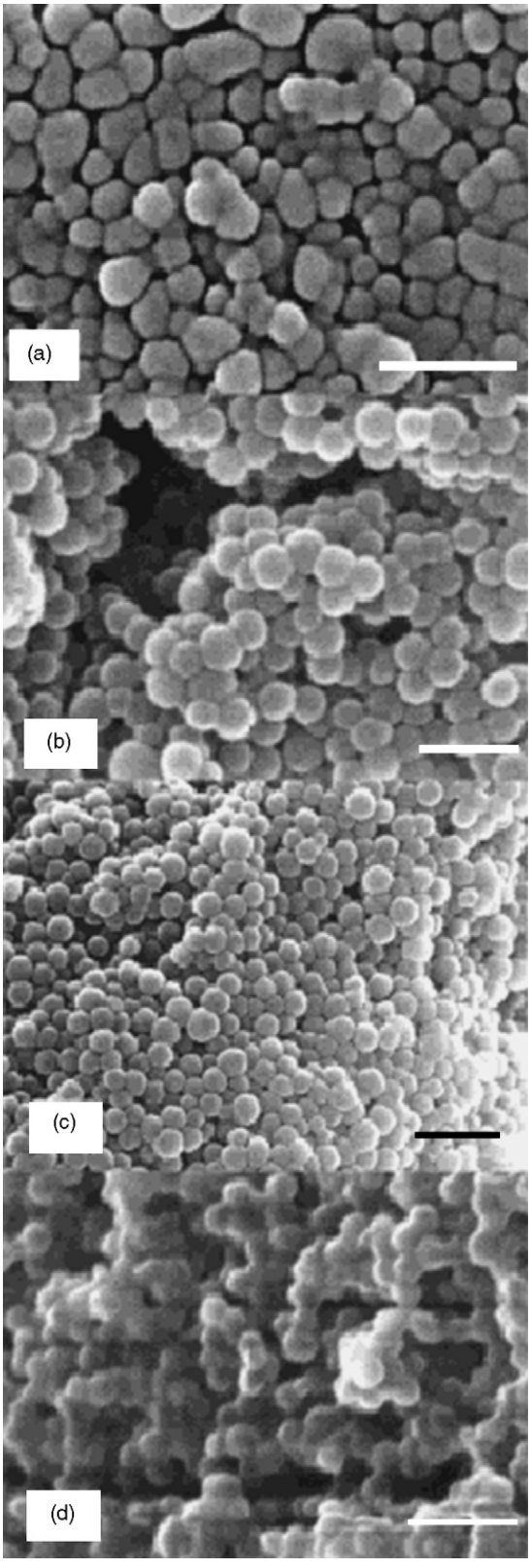

Fig. 7. SEM images of zinc ferrite–silica nanoparticles, where (a, b, c and d) refer to AOT, AOT/Brij 30, Brij 30 and SDS/propanol in *n*-heptane microemulsions, respectively, and the bar corresponds to 150 nm. Reprinted with permission from [59], copyright (2002) American Chemical Society.

cursor cations in the form of divalent hydroxides, the resulting powder was primarily made up of goethite (α-FeOOH). In other words, if the pH value of the precipitation was below 8, goethite was formed, whereas if the pH of the precipitation was higher than 8, a spinel phase with better crystallinity was obtained. The powders synthesized between precipitating pH values of 8 and 10 were found to have average particle sizes in the order of 2–3 nm, whereas powders synthesized at pH values higher than 10 had average particle sizes of approximately 4 nm. This size of the produced particles is consistent with the estimated diameters of the reverse micelles, i.e., the water content used in this microemulsion system. The pH also affected the shape of the nanoparticles. At lower pH values, close to 10, the nanoparticles showed partly acicular nature. On the other hand, particles synthesized at higher pH values, close to 13, were spherical and of uniform size. This was explained by the existence of worm-like reverse micelles, together with the spherical micelles, so that the former gave rise to acicular particles, while the latter micelles induced the formation of spherical particles.

5.3. Manganese–zinc (Mn–Zn) ferrite

Ferrites $Zn_xMn_{1-x}Fe_2O_4$ ($0 \leq x \leq 1$) has a crystalline structure of spinel type. In spinels the unit cell is of face-centered cubic symmetry. The unit cell (with rib length $d \approx 0.84$ nm) is formed by 32 oxygen atoms and 24 cations. There are 64 tetrahedral and 32 octahedral possible positions for cations in the unit cell. Only 8 tetrahedral and 16 octahedral positions are occupied by the cations. They are named A and B-positions, respectively. Mn–Zn ferrites as magnetic materials are widely used for cores of intermediate frequency transformers, inductors, loudspeakers and other electromagnetic devices. They are distinguished for their low Curie temperatures, low remaining magnetization and low values of the magnetic crystalline anisotropy constant. Another important use of Mn–Zn ferrites is in the development of electric vehicles.

Automakers are actively researching the development of electric vehicles (EV), hybrid electric vehicles and fuel cell vehicles for protecting the global environment in the 21st century. There are two major methods of charging automobiles: the inductive charging system (ICS) and the conductive charging system. An ICS incorporates a connector, which divides the primary and secondary coils in a transformer and adopts a high-frequency switching circuitry operated between 100 and 370 kHz [62]. Mn–Zn ferrite cores are known to be most suitable for this frequency range. The ICS-use ferrite cores need to have a low-loss characteristic to minimize heat generation during charging and high saturation induction characteristic to cope with large input currents.

Mn–Zn ferrite nanoparticles have been synthesized by precipitating Mn^{2+}, Zn^{2+} and Fe^{3+} hydroxides in a microemulsion followed by the calcination of hydroxide precursors [63]. Nanocrystalline Mn–Zn ferrite particles ($Mn_{0.5}Zn_{0.5}Fe_2O_4$) were prepared with precipitation in the reverse microemulsion consisting of 1-hexanol as an oil phase, hexadecyltrimethylethyl ammonium bromide (CTAB) as the surfactant, 1-butanol as the co-surfactant and an aqueous phase [64]. The application of 1-

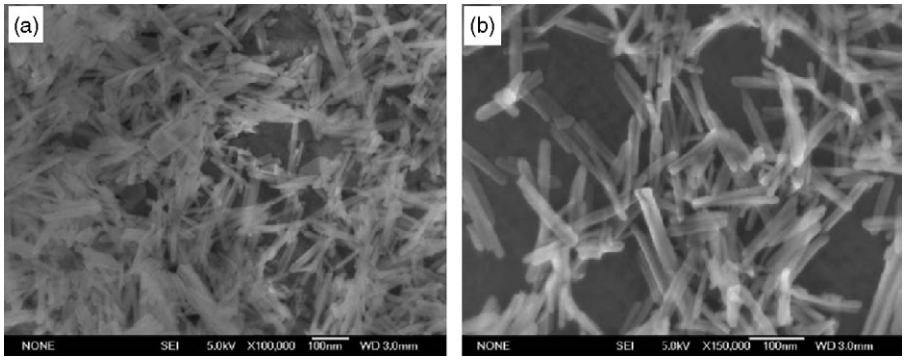

Fig. 8. SEM images of the synthesized nanorods taken at different magnifications. Reprinted with permission from [70].

butanol as a co-surfactant expanded the microemulsions stability region, which made it possible to obtain more nanoparticles as well as a larger particle size. The particle size of the prepared samples was in the range 3.5–8.5 nm and it was observed that the particle size increased with increasing water content. The nanoparticles obtained by this method were crystalline and spherical in shape.

5.4. Cobalt ferrites ($CoFe_2O_4$)

Cobalt ferrite, with a partially inverse spinel structure, is one of the most important and most abundant magnetic materials. As a conventional magnetic material, with a Curie temperature (T_c) about 793 K, $CoFe_2O_4$ is well known to have large magnetic anisotropy, moderate saturation magnetization, remarkable chemical stability and a mechanical hardness, which make it a good candidate for the recording media. Cobalt ultrafine powders [32,65] and films [66,67] have attracted considerable attention for their wide range of technological applications such as transformer cores, recording heads, antenna rods, memory, ferrofluids, biomedical application, sensors, etc. [68,69].

A simple synthesis route, the CTAB-assisted hydrothermal method, was used to fabricate single-crystalline phase $CoFe_2O_4$ nanorods having diameters of 25 nm and lengths up to 120 nm (Fig. 8) [70]. The magnetization of the $CoFe_2O_4$ nanorods is lower than that of the $CoFe_2O_4$ nanoparticles, attributed to the spatial confinement effects and high shape anisotropy. It was shown that the surfactant CTAB played a key role in controlling the nucleation and growth of the $CoFe_2O_4$ nanorods. For the reaction system in the presence of CTAB, the surface tension of solution is reduced due to the presence of surfactant, which lower the energy needed for the formation of a new phase. CTAB is an ionic compound, which ionizes completely in water [71]. The resulting CTA^+ is a positively charged tetrahedron with a long hydrophobic tail, while the growth unit for $CoFe_2O_4$ crystal is considered to be $Co–Fe–OH^-$. Therefore, ion pairs between CTA^+ and $Co–Fe–OH^-$ could be formed due to electrostatic interaction. The $Co–Fe–OH^-$ particles are negatively charged, and so CTA^+ ions were adsorbed on the particle surface to form a film. The film is assembled and floatable. When the surfactant molecule leaves, $Co–Fe–OH^-$ will be carried away in the form of ion pairs, in the crystallization process. The surfactant molecule here acts as both, a growth controller as well as an agglomeration inhibitor, by forming a film covering on the newly formed $CoFe_2O_4$ crystal. Thus, the formation mechanism of the $CoFe_2O_4$ nanorods has been explained as the adsorption of CTA^+, which affected the growth rate and orientation of crystals. This method is thus expected to be a promising technique to fabricate one-dimensional nanostructures of other magnetic materials also.

The magnetic characteristics of particle used for recording media depend crucially on their size and shape. For any magnetic material there exists a critical size, d_{SD}, below which it remains single domain. There also exist a characteristic size of the parti-

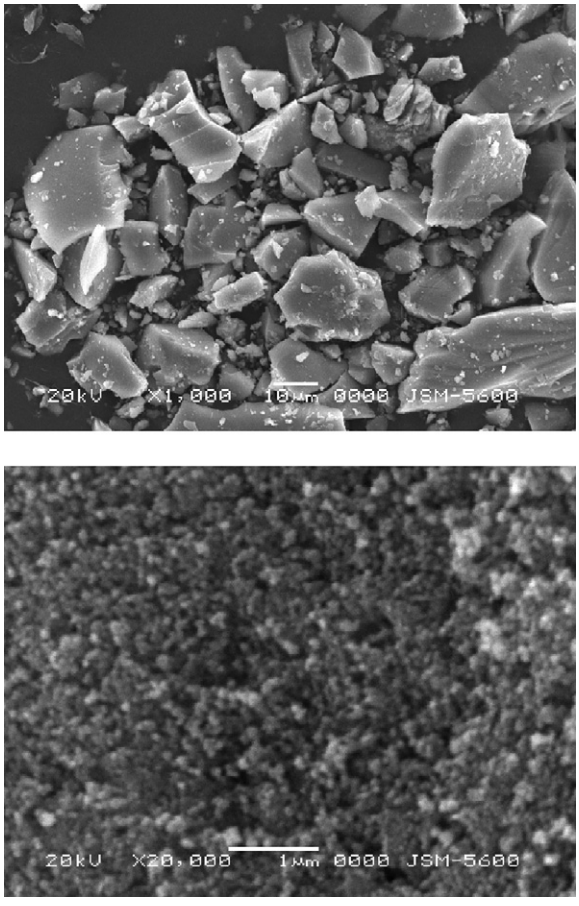

Fig. 9. SEM images of cobalt ferrite at different magnifications. Reprinted with permission from [77].

cle, d_{Sp}, below which the material becomes superparamagnetic at the temperature of operation, i.e., no hysteresis, zero coercivity and zero remanence at the temperature of operation. Therefore, the size range over which a magnetic particle is useful in a storage medium is $d_{Sp} < d < d_{SD}$ [72]. Magnetic nanoparticles of cobalt ferrite have been synthesized using water-in-oil microemulsion consisting of water, cetyltrimethylammonium bromide (surfactant), *n*-butanol (co-surfactant) and *n*-octane (oil). Precursor hydroxides were precipitated in the aqueous cores of water-in-oil microemulsions and these were then separated and calcined to give the magnetic oxide. These nanoparticles were less than 50 nm in size and a high intrinsic coercivity (1440 Oe) and saturation magnetization (65 emu/g) [32]. The calcined particles showed agglomerates of particles less than 50 nm in size. Since these particles are smaller than the critical domain size (d_{SD}) for cobalt ferrite [73], all particles are single domain in size. Thus, this method led to the synthesis of high coercivity cobalt ferrites with single-domain particles and no non-magnetic impurities. The enhancement in coercivity due to the addition of cobalt arises from the increase in magnetocrystalline anisotropy imparted by cobalt to the oxide.

A reverse micellar system of AOT/isooctane was used to produce nanoparticles of $CoFe_2O_4$ with particle size ranging from 15 to 150 nm [74]. $FeSO_4{\cdot}7H_2O$ and $CoSO_4{\cdot}7H_2O$ were the metal salt reactants and NH_4OH was the reducing agent used in the reaction. The molar concentration of $FeSO_4{\cdot}7H_2O$ was found to be an important parameter in control of nanoparticle size. A decrease in the concentration of $FeSO_4{\cdot}7H_2O$ resulted in larger $CoFe_2O_4$ particles. This may be because of the increase in the production of reverse micelles in the inter-phase due to increasing percentage of $FeSO_4$. In other words, the percent of particles may be increased, but the particle size will be decreased.

Nanoparticles of $CoFe_2O_4$ has also been synthesized using sodium dodecylsulfate (SDS) as a surfactant. $CoFe_2O_4$ spinel ferrite nanoparticle was prepared by using a microemulsion method in which the reagents $CoCl_2{\cdot}6H_2O$ and $FeCl_2{\cdot}4H_2O$ were mixed in an aqueous solution [75]. An aqueous surfactant with 0.03 mol SDS was added to form a mixed micellar solution of $Co(DS)_2$ and $Fe(DS)_2$. The nanoparticles were formed by the addition of methylamine to this solution at 323 K. The $CoFe_2O_4$ nanoparticles formed had a mean size of 12 nm. The neutron diffraction studies and temperature dependent decay of magnetization showed superparamagnetic relation occurring in these nanoparticles.

Microemulsion method has produced high-quality $CoFe_2O_4$ nanoparticles with a size distribution of about 15% or less. Since one of the starting reagents is chemically unstable ferrous salt, the synthesis process is complicated and extra caution has to be exercised in order to obtain consistent products. $CoFe_2O_4$

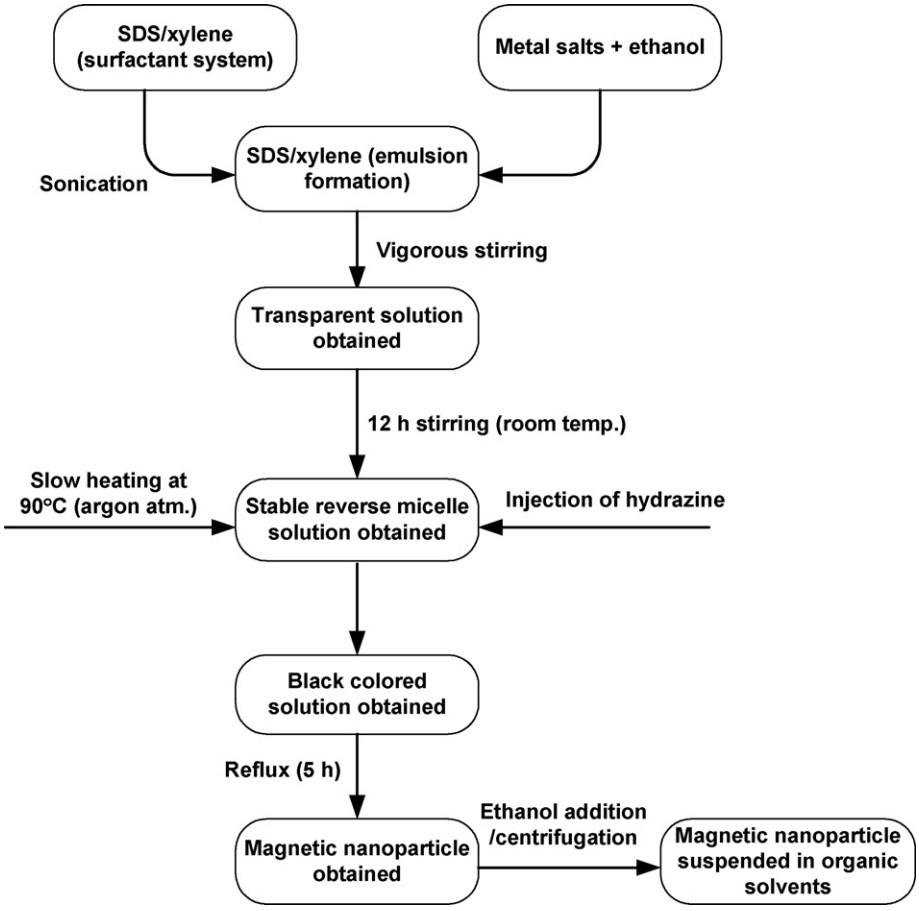

Fig. 10. Experimental procedures for the synthesis of ferrite nanoparticles.

nanoparticles were synthesized by using a stable ferric salt of $FeCl_3$ with a micellar microemulsion method. The normal micelles were formed by SDS in aqueous solutions. The mean size of the nanoparticles can be controlled from less than 4 to about 10 nm through controlling the concentrations of the reagents. Magnetic measurements and neutron diffraction studies demonstrate the superparamagnetic nature of these $CoFe_2O_4$ nanoparticles. The blocking temperature and coercive field of the nanoparticles increased with increasing size of the nanoparticles [76]. Recently, a new inverse microemulsion containing a zwitterionic surfactant, cetyltrimethylammonium *p*-toluene sulfonate was used to prepare the nanoparticles of mixed transition-metal spinel oxide, $CoFe_2O_4$. The prepared nanoparticles had an average crystalline size of 20–40 nm (Fig. 9) [77].

6. Large-scale synthesis of spinel ferrites

For many applications, the synthesis of uniformly sized nanoparticles is of key importance, because the electrical, optical and magnetic properties of these nanoparticles depend strongly on their dimensions. Even though highly crystalline and uniformly sized magnetic nanoparticles have been produced, these synthetic procedures cannot be applied to large-scale and economic production, because they require expensive and often toxic reagents, more complicated synthetic steps, and high reaction temperature. In an attempt for large-scale nanoparticle production, uniformly sized and highly crystalline magnetite nanoparticles were synthesized from the high temperature reaction of inexpensive and non-toxic iron salts in reverse micelles [78]. The key feature of current synthetic procedure is the maintenance of the micelle structure during the formation of the nanoparticles at high reaction temperature. Under optimized reaction conditions, several grams of nanoparticles were synthesized in a single reaction without going through a size selection process. Also, particle size can be simply controlled by varying the relative concentrations of metal salt and surfactant.

Large-scale synthesis of several mixed metal ferrites of cobalt ferrite, manganese ferrite, nickel ferrite and zinc ferrite were prepared as shown in Fig. 10. One remarkable feature of this synthetic procedure was that the relative amount of organic solvent was much less than that used in the conventional nanoparticle synthesis using reverse micelle. In other words, the concentration of the reactants was 3–10 times higher than that of the conventional synthesis, yielding a much greater quantity of nanoparticles for the same amount of solvent, which is very important for the large-scale production of nanoparticles. The nanoparticles were synthesized using reverse micelles as nanoreactors under reflux conditions. Also, even though the reaction mixture was refluxed for 5 h, the synthesized nanoparticles were non-aggregated and well dispersed.

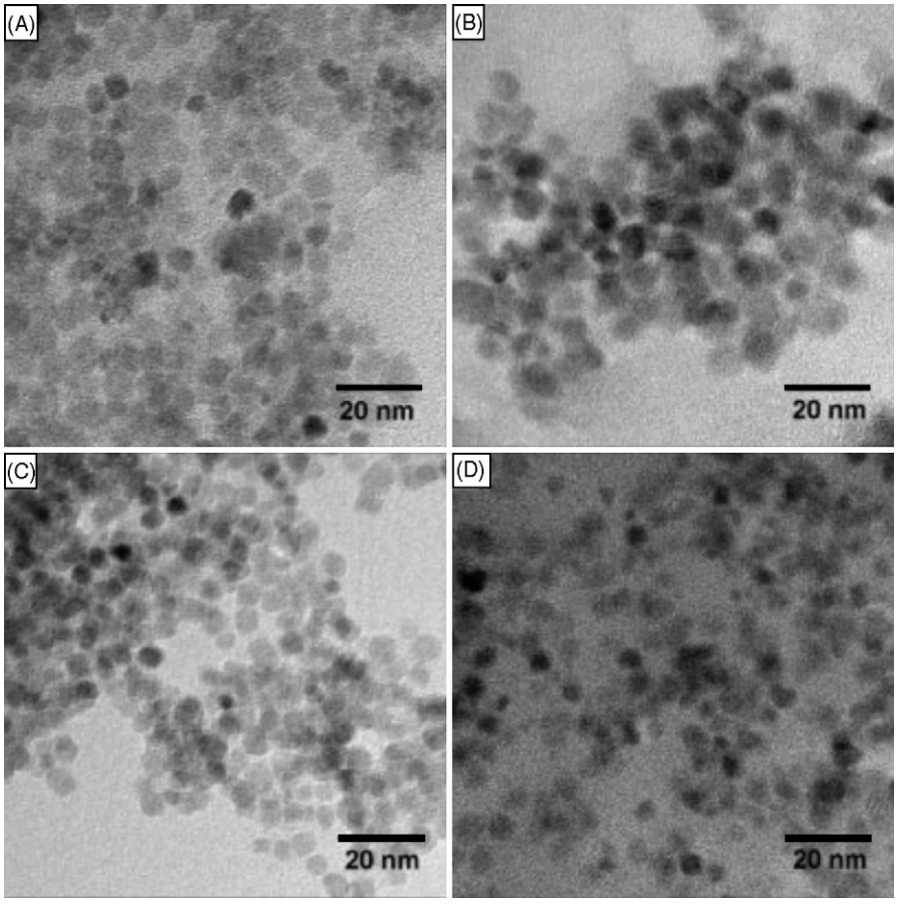

Fig. 11. TEM images of metal ferrite nanoparticles: (A) cobalt ferrite, (B) manganese ferrite, (C) nickel ferrite and (D) zinc ferrite. Reprinted with permission from [78].

Table 3
Metal salts used in the synthesis of mixed metal ferrite nanoparticles and elemental analysis results of these nanoparticles

Ferrites	Metal salts	Size (nm)	Me^{2+}/Fe^{3+} (EDS)	Me^{2+}/Fe^{3+} (ICP-AES)
Cobalt	$Co(NO_3)_2{\cdot}6H_2O$	6.5	0.87:2	0.85:2
Manganese	$MnCl_4{\cdot}4H_2O$	8	1.1:2	1.1:2
Nickel	$Ni(CH_3COO)_2{\cdot}4H_2O$	5.5	0.97:2	0.99:2
Zinc	$Zn(NO_3)_2{\cdot}6H_2O$	4	0.89:2	0.88:2

In addition the as-synthesized nanoparticles were highly crystalline, which eliminated the need for post-thermal treatment to crystallize the nanoparticles. Various metal salts with different anion such as chloride, nitrate, sulfate and acetate were used to synthesize ferrite nanoparticles. Control of the average diameter was also possible by adjusting the amount of surfactant, concentration of metal salts and W_0 ratio (molar ratio of water to surfactant). Table 3 summarizes the metal precursors used in the synthesis.

TEM images showed that all the prepared nanoparticles had uniform size distribution, inspite of being produced without any size selection process (Fig. 11). Also the particles were shown to exhibit inverse spinel structures of metal ferrites (XRD analysis). The elemental analysis of these nanoparticles, using ICP-AES and energy-dispersive X-ray spectroscopy (EDX), showed that the molar ratio of Fe^{3+}/Me^{2+} was close to 2. These results on the synthesis of nanoparticles of mixed metal ferrites are important because the composition of the ferrite nanoparticles can be tuned by simply changing the composition of the metal salts.

7. Conclusions

The design and synthesis of inorganic materials with nanosized dimensions has been made possible because of the ability of surfactants to self-assemble into well-defined structures. The structures formed by self-assembly of the surfactant are used as a kind of template for the synthesis. Precipitation in a water-in-oil microemulsion has been shown to be a very promising technique for preparing monodispersed, ultrafine particles of controlled size and morphology. With this method, the co-precipitation occurs in tiny droplets of aqueous phase that are embedded with a surfactant, so-called reverse micelles, which are distributed in an oil phase. The water pools of reverse micelles act as microreactors for the synthesis of the particles. The particle size of the product depends on the size of these water pools. It has also been proved that the concentrations of the reactants in the aqueous solution of reverse micelles also influence the size of the product particles. Reverse micellar techniques have several additional parameters, which offer powerful options for the fabrication of nanoparticles in a softer, less harsh environment, compared to other methods of producing nanoparticles. The tailoring of the nanoparticles is most common in the size and size distribution, but crystal structure, and cation occupancy have also been demonstrated.

The microemulsion methods have led to the synthesis of single-phase nanosized ferrites at room temperature without requiring subsequent firing of the materials. The synthetic procedure of ferrites from microemulsions provides various advantages. First, the synthetic process is economical and environmentally friendly because it involves inexpensive and less toxic iron salts and a reduced amount of organic solvent. Second, uniform and highly crystalline nanoparticles were produced without going through any size-selection process or post-synthetic heat treatment. Third, nanoparticles could be produced on a multigram scale in a single reaction and the indications are that scale-up can be achieved relatively easily.

References

[1] B.H. Sohn, R.E. Cohen, Processible optically transparent block copolymer films containing superparamagnetic iron oxide nanoclusters, Chem. Mater. 9 (1997) 264–269.
[2] Y.I. Kim, D. Kim, C.S. Lee, Synthesis and characterization of $CoFe_2O_4$ magnetic nanoparticles prepared by temperature-controlled coprecipitation method, Physica B 337 (2003) 42–51.
[3] C. Caizer, M. Popovici, C. Savii, Spherical $(Zn_\delta Ni_{1-\delta}Fe_2O_4)_\gamma$ nanoparticles in an amorphous $(SiO_2)_{1-\gamma}$ matrix, prepared with the sol–gel method, Acta Mater. 51 (2003) 3607–3616.
[4] D.K. Kim, Y. Zhang, W. Voit, K.V. Rao, M. Muhammed, Synthesis and characterization of surfactant-coated superparamagnetic monodispersed iron oxide nanoparticles, J. Magn. Magn. Mater. 225 (2001) 30–36.
[5] J.A.L. Perez, M.A.L. Quintela, J. Mira, J. Rivas, S.W. Charles, Advances in the preparation of magnetic nanoparticles by the microemulsion method, J. Phys. Chem. B 101 (1997) 8045–8047.
[6] Q. Chen, Z.J. Zhang, Size-dependent superparamagnetic properties of $MgFe_2O_4$ spinel ferrite nanocrystallites, Appl. Phys. Lett. 73 (1998) 3156–3158.
[7] Z.X. Tang, C.M. Sorensen, K.J. Klabunde, G.C. Hadjipanayis, Preparation of Mn ferrite fine particles from aqueous solution, J. Colloid Interface Sci. 146 (1991) 38–46.
[8] C.T. Seip, E.E. Carpenter, C.J. O'Connor, V.T. John, S. Li, Magnetic properties of a series of ferrite nanoparticles synthesized in reverse micelles, IEEE Trans. Magn. 34 (1998) 1111–1113.
[9] J.F. Hochepied, P. Bonville, M.P. Pileni, Nonstoichiometric zinc ferrite nanocrystals: syntheses and unusual magnetic properties, J. Phys. Chem. B 104 (2000) 905–912.
[10] C. Liu, B. Zou, A.J. Rondinone, Z.J. Zhang, Reverse micelle synthesis and characterization of superparamagnetic $MnFe_2O_4$ spinel ferrite nanocrystallites, J. Phys. Chem. B 104 (2000) 1141–1145.
[11] C. Chen, Magnetism and Metallurgy of Soft Magnetic Materials, Dover Publications, Inc., New York, 1986.
[12] C.M. Sorensen, in: K.J. Klabunde (Ed.), Nanoscale Materials in Chemistry, Wiley, New York, 2001.
[13] A.H. Morrish, The Physical Principles of Magnetism, Wiley, New York, 1965.
[14] E.C. Stoner, E.P. Wohlfarth, A mechanism of magnetic hysteresis in heterogeneous alloys, Philos. Trans. R. Soc. A240 (1948) 599–642.
[15] D.L. Leslie-Pelecky, R.D. Rieke, Magnetic properties of nanostructured materials, Chem. Mater. 8 (1996) 1770–1783.
[16] C.R. Vestal, J.Z. Zhang, Magnetic spinel ferrite nanoparticles from microemulsions, Int. J. Nanotechnol. 1 (2004) 240–263.
[17] L. Neel, Magnetic properties of ferrites: ferrimagnetism and antiferromagnetism, Ann. Phys. Paris 3 (1948) 137–198.

[18] H.S.C. O'Neill, A. Navrotsky, Simple spinels: crystallographic parameters, cation radii, lattice energies, and cation distribution, Am. Mineral. 69 (1983) 181–194.
[19] H.B. Callen, S.E. Harrison, C.J. Kriessman, Cation distribution in ferrospinels, Theor. Phys. Rev. 103 (1956) 851–856.
[20] D.C. Jiles, Introduction to Magnetism and Magnetic Materials, second ed., Chapman & Hall, London, 1991.
[21] E.C. Snelling, Soft Ferrites: Properties and Applications, second ed., Butterworths Publishing, 1989.
[22] T. Hyeon, Y. Chung, J. Park, S.S. Lee, Y.W. Kim, B.H. Park, Synthesis of highly crystalline and monodisperse cobalt ferrite nanocrystals, J. Phys. Chem. B 106 (2002) 6831–6833.
[23] M. Kagawa, M. Kikuchi, R. Ohno, T. Nagae, Stability of ultrafine tetragonal ZrO2 coprecipitated with Al_2O_3 by the spray-ICP technique, J. Am. Ceram. Soc. 66 (1983) 751–754.
[24] M.A. Blesa, C. Matijevic, Phase transformations of iron oxides, oxohydroxydes and hydrous oxides in aqueous media, Adv. Colloid Interface Sci. 29 (1989) 173–221.
[25] G. Xiong, Z. Mai, M. Xu, S. Cui, Y. Ni, Z. Zhao, X. Wang, L. Lu, Preparation and magnetic properties of $CoCrFeO_4$ nanocrystals, Chem. Mater. 13 (2001) 1943–1945.
[26] L.J. Cote, A.S. Teja, A.P. Wilkinson, Z.J. Zhang, Continuous hydrothermal synthesis and crystallization of magnetic oxide nanoparticles, J. Mater. Res. 17 (2002) 2410–2416.
[27] Q. Chen, A.J. Rondinone, B.C. Chakoumakos, Z.J. Zhang, Synthesis of superparamagnetic $MgFe_2O_4$ nanoparticles by co-precipitation, J. Magn. Magn. Mater. 194 (1999) 1–7.
[28] Z.J. Zhang, Z.L. Wang, B.C. Chakoumakos, J.S. Yin, Temperature dependence of cation distribution and oxidation state in magnetic Mn–Fe ferrite nanocrystals, J. Am. Chem. Soc. 120 (1998) 1800–1804.
[29] A. Cabanas, M. Poliakoff, The continuous hydrothermal synthesis of nanoparticulate ferrites in near critical and supercritical water, J. Mater. Chem. 11 (2001) 1408–1416.
[30] M. Boutonnet, J. Kizling, P. Stenius, G. Marie, The preparation of monodisperse colloidal metal particles from microemulsions, Colloid Surf. 5 (1982) 209–225.
[31] M.P. Pileni, in: J.H. Fendler (Ed.), Nanoparticles and Nanostructures Films, Wiley-VCH, Weinheim, 1997.
[32] V. Pillai, D.O. Shah, Synthesis of high-coercivity cobalt ferrite particles using water-in-oil microemulsions, J. Magn. Magn. Mater. 163 (1996) 243–248.
[33] Y. Li, C.W. Park, Particle size distribution in the synthesis of nanoparticles using microemulsions, Langmuir 15 (1999) 952–956.
[34] A. Lattes, I. Rico, A. de Savignac, A. Samii, Reactivity in anisotropic media, Tetrahedron 43 (1987) 1725–1729.
[35] D.J. Mitchell, B.W.J. Ninham, Micelles, vesicles and microemulsions, J. Chem. Soc. Faraday Trans. II 77 (1981) 601–629.
[36] B.K. Paul, S.P. Moulik, Microemulsions: an overview, J. Dispers. Sci. Technol. 18 (1997) 301–367.
[37] I. Capek, Preparation of metal nanoparticles in water-in-oil (w/o) microemulsions, Adv. Colloid Interface Sci. 110 (2004) 49–74.
[38] J.P. Chen, K.M. Lee, C.M. Sorensen, K.J. Klabunde, G.C. Hadjipanyis, Magnetic properties of microemulsion synthesized cobalt fine particle, J. Appl. Phys. 75 (1994) 5876–5878.
[39] M. Gobe, K. Kon-No, K. Kandori, A. Kitahara, Preparation and characterization of monodisperse magnetite sols in w/o microemulsion, J. Colloid Interface Sci. 93 (1983) 293–295.
[40] M. Boutonnet, J. Kizling, R. Touroude, G. Marie, P. Stenius, Monodispersed colloidal metal particles from nonaqueous solutions: catalytic behavior in hydrogenolysis and isomerization of hydrocarbons of supported platinum particles, Catal. Lett. 9 (1991) 347–354.
[41] K. Holmberg, Surfactant-template nanomaterials synthesis, J. Colloid Interface Sci. 274 (2004) 355–364.
[42] M.P. Pileni, The role of soft colloidal templates in controlling the size and shape of inorganic nanocrystals, Nat. Mater. 2 (2003) 145–150.
[43] A. Courty, I. Lisiecki, M.P. Pileni, Vibration of self-organized silver nanocrystals, J. Chem. Phys. 116 (2002) 8074–8078.
[44] P.D.I. Fletcher, B.H. Robinson, R.B. Freedman, C.J. Oldfield, Activity of lipase in water-in-oil microemulsions, J. Chem. Soc. Faraday Trans. I 81 (1985) 2667–2679.
[45] M.P. Pileni, Nanosized particles made in colloidal assemblies, Langmuir 13 (1997) 3266–3276.
[46] H. Althues, S. Kaskel, Sulfated zirconia nanoparticles synthesized in reverse microemulsions: preparation and catalytic properties, Langmuir 18 (2002) 7428–7435.
[47] A.E.C. Palmqvist, Synthesis of ordered mesoporous materials using surfactant liquid crystals or micellar solutions, Curr. Opin. Colloid Interface Sci. 8 (2003) 145–155.
[48] C. Tojo, M.C. Blanco, M.A. Lopez-Quintela, Preparation of nanoparticles in microemulsions: a Monte Carlo study of the influence of the synthesis variables, Langmuir 13 (1997) 4527–4534.
[49] M.A. Lopez-Quintela, C. Tojo, M.C. Blanco, L. Garcia Rio, J.R. Leis, Microemulsion dynamics and reactions in microemulsions, Curr. Opin. Colloid Interface Sci. 9 (2004) 264–278.
[50] S. Quintillan, C. Tojo, M.C. Blanco, M.A. Lopez-Quintela, Effects of the intermicellar exchange on the size control of nanoparticles synthesized in microemulsions, Langmuir 17 (2001) 7251–7254.
[51] K. Osseo-Karare, F.J. Arrigada, Growth kinetics of nanosized silica in a nonionic water-in-oil microemulsion: a reverse micellar pseudo-phase reaction model, J. Colloid Interface Sci. 218 (1999) 68–76.
[52] F. Burghart, W. Potzel, G. Kalvius, E. Schreier, G. Grosse, D. Noakes, W. Schafer, W. Kockelmann, S. Campbell, W. Kaczmarek, A. Martin, M. Krause, Magnetism of crystalline and nanostructured $ZnFe_2O_4$, Physica B 289–290 (2000) 286–290.
[53] J.C. Ho, H. Hamdeh, Y. Chen, S. Lin, Y. Yao, R. Willey, S. Oliver, Low-temperature calorimetric properties of zinc ferrite nanoparticles, Phys. Rev. B 52 (1995) 10122–10126.
[54] M. Anantharaman, S. Jagathesan, K. Malini, S. Sindhu, A. Narayanaswamy, C. Chinnasamy, J. Jacobs, S. Reijne, K. Seshan, R. Smits, H.J. Brongerma, On the magnetic properties of ultra-fine zinc ferrites, J. Magn. Magn. Mater. 189 (1998) 83–88.
[55] A.P. Homola, M.R. Lorentz, H. Suusner, S. Rice, Ultrathin particulate magnetic recording media, J. Appl. Phys. 61 (1987) 3898–3901.
[56] A.P. Philips, M.P.B. van Brugge, C. Pathmamanoharan, Magnetic silica dispersions: preparation and stability of surface-modified silica particles with a magnetic core, Langmuir 10 (1994) 92–99.
[57] M. Klotz, A. Ayral, C. Guizard, C. Menager, V.J. Cabuil, Silica coating on colloidal maghemite particles, J. Colloid Interface Sci. 220 (1999) 357–361.
[58] P. Komar, in: K.L. Mittal (Ed.), Handbook of Microemulsion Science and Technology, Marcel Dekker, New York, 1999.
[59] F. Grasset, N. Labhsetwar, D. Li, D.C. Park, N. Saito, H. Haneda, O. Cador, T. Roisnel, S. Mornet, E. Duguet, J. Portier, J. Etourneau, Synthesis and magnetic characterization of zinc ferrite nanoparticles with different environments: powder, colloidal solution, and zinc ferrite–silica core–shell nanoparticles, Langmuir 18 (2002) 8209–8216.
[60] S.A. Morrison, C.L. Cahill, S. Calvin, R. Swaminathan, M.E. Mchenry, V.G. Harris, Magnetic and structural properties of nickel zinc ferrite nanoparticles synthesized at room temperature, J. Appl. Phys. 95 (2004) 6392–6395.
[61] V. Uskokovic, M. Drofenik, I. Ban, Characterization of nanosized nickel–zinc ferrites synthesized within reverse micelles of CTAB/1-hexanol/water microemulsions, J. Magn. Magn. Mater. 284 (2004) 294–302.
[62] D. Ouwerkerk, T. Sekimori, H. Satoh, New inductive charging approach, Jeva Electric Vehicle Forum (1998) 181.
[63] D.O. Yener, H. Giesche, Synthesis of pure and manganese-, nickel-, and zinc-doped ferrite particles in water-in-oil microemulsions, J. Am. Ceram. Soc. 84 (2001) 1987–1990.
[64] A. Kosak, D. Makovec, M. Drofenik, Preparation of MnZn-ferrite nanoparticles in a water/CTAB, 1-butanol/1-hexanol reverse microemulsion, Phys. Stat. Sol. C1 12 (2004) 3521–3524.
[65] S.W. Charles, K.J. Davies, S. Wells, R.V. Upadhyay, K. OGrady, M. El Hilo, T. Meaz, S. Morup, The observation of multi-axial anisotropy in ultrafine cobalt ferrite particles used in magnetic fluids, J. Magn. Magn. Mater. 149 (1995) 14–18.

[66] J.W.D. Martens, W.L. Eeters, H.M. van Noort, M. Errnan, Optical, magnetio-optical and Mossbauer spectroscopy on Co^{3+}-substituted cobalt ferrite $Co^{2+}Fe_{2-x}Co^{3+}{}_xO_4$, J. Phys. Chem. Solids 46 (1985) 411–418.
[67] S.N. Okuno, S. Hashimoto, K. Inomata, Preferred crystal orientation of cobalt ferrite thin films induced by ion bombardment during deposition, J. Appl. Phys. 71 (1992) 5926–5929.
[68] F. Bodkar, S. Morup, S. Linderoth, Surface effects in metallic iron nanoparticles, Phys. Rev. Lett. 72 (1994) 282–285.
[69] C.V. Gopal Reddy, S.V. Manorama, V.J. Rao, Preparation and characterization of ferrite as gas sensor materials, J. Mater. Sci. Lett. 19 (2000) 775–778.
[70] G.B. Ji, S.L. Tang, S.K. Ren, F.M. Zhang, B.X. Gu, Y.W. Du, Simplified synthesis of single-crystalline magnetic $CoFe_2O_4$ nanorods by a surfactant-assisted hydrothermal process, J. Cryst. Growth 270 (2004) 156–161.
[71] L. Yan, Y.D. Li, Z.X. Deng, J. Zhuang, X. Sun, Surfactant-assisted hydrothermal synthesis of hydroxyapatite nanorods, Int. J. Inorg. Mater. 3 (2001) 633–637.
[72] D.J. Craik, in: D.J. Craik (Ed.), Magnetic Oxides Part I, Wiley Interscience, New York, 1975.
[73] G. Bate, in: D.J. Craik (Ed.), Magnetic Oxides Part II, Wiley Interscience, New York, 1975.
[74] O. Doker, E. Bayraktar, U. Mehmetoglu, A. Calimli, Production of iron–cobalt compound nanoparticles using reverse micellar system, Rev. Adv. Mater. Sci. 5 (2003) 498–500.
[75] A.J. Rondinone, A.C. Samai, Z.J. Zhang, Superparamagnetic relaxation and magnetic anisotropy energy distribution in $CoFe_2O_4$ spinel ferrite nanocrystallites, J. Phys. Chem. B 103 (1999) 6876–6880.
[76] C. Liu, A.J. Rondinone, Z.J. Zhang, Synthesis of magnetic spinel ferrite $CoFe_2O_4$ nanoparticles from ferric salt and characterization of the sized-dependent superparamagnetic properties, Pure Appl. Chem. 72 (2000) 37–45.
[77] D.S. Mathew, R.S. Juang, Preparation of cobalt ferrite and metal oxide nanoparticles in microemulsions of cetyltrimethylammonium *p*-toluene sulfonate, J. Chin. Inst. Chem. Eng. 37 (2006) 305–309.
[78] Y. Lee, J. Lee, C.J. Bae, J.G. Park, H.J. Noh, J.H. Park, T. Hyeon, Large-scale synthesis of uniform and crystalline magnetite nanoparticles using reverse micelle as nanoreactors under reflux conditions, Adv. Funct. Mater. 15 (2005) 503–509.